RSC Advances

PAPER

View Article Online
View Journal | View Issue

Cite this: *RSC Adv.*, 2017, **7**, 24418

Facile and controllable synthesis of solid $Co_3V_2O_8$ micro-pencils as a highly efficient anode for Li-ion batteries†

Jian Yang, ‡ Mengqiang Wu,* Feng Gong, ‡* Tingting Feng, Cheng Chen and Jiaxuan Liao

Received 16th March 2017
Accepted 26th April 2017

DOI: 10.1039/c7ra03118a

rsc.li/rsc-advances

Mixed metal vanadate oxides are promising superior anode materials for lithium ion batteries due to their high specific capacities, improved cycling performance and excellent rate properties. In this work, we demonstrate a facile and controllable synthesis of solid $Co_3V_2O_8$ micro-particles with different morphologies through a hydrothermal method. By controlling the reaction time, either $Co_3V_2O_8$ micro-plates or micro-pencils could be fabricated. Characterization *via* X-ray diffraction (XRD) and transmission electron microscopy (TEM) demonstrated the pure phase and solid morphology of the $Co_3V_2O_8$ micro-pencils. Scanning electron microscopy (SEM) images of the products obtained at different stages clearly revealed the formation process of the $Co_3V_2O_8$ micro-pencils. Electrochemical measurements of the $Co_3V_2O_8$ micro-pencils showed an excellent lithium storage capacity (1137 mA h g^{-1} at 200 mA g^{-1}), good cycling retention (~670 mA h g^{-1} after 330 cycles), desirable coulombic efficiency (~100% for 350 cycles) and notable rate capability (300 mA h g^{-1} at 2000 mA g^{-1}). The improved electrochemical performances of the solid $Co_3V_2O_8$ micro-pencils indicate their great potential as high-performance anode materials for lithium ion batteries.

Introduction

Transition metal oxides for anode materials of lithium-ion batteries (LIBs) have attracted much attention owing to their high capacities, eminent initial coulombic efficiencies, and enhanced cycling performance.[1–4] However, they may undergo various problems such as volume expansion and capacity fading[5,6] which limit their practical application. Therefore, the morphology and particle size of the transition metal oxides need to be carefully designed and modulated[7–11] to solve the above issues. Recently, researchers have reported that mixed metal oxides might have better electrochemical performance than single-phase metal oxides, with features such as higher ionic and electrical conductivity, enhanced reversible capacity and improved mechanical stability,[12–15] which could be attributed to the interfacial effects and the synergistic effects of mixed cation species in the mixed metal oxides.[16]

Among various diverse mixed metal oxides, metal vanadates have attracted a lot of interest for their unique morphology and prominent electrochemical properties.[17–24] For instance, through a simple solvothermal method, Yin *et al.* successfully synthesized MoV_2O_8 nanorods,[18] which exhibited excellent specific capacity (over 1325 mA h g^{-1} after 50 cycles at 0.2 A g^{-1}), high rate performance (a high specific capacity of 570 mA h g^{-1} at a current density of 10.0 A g^{-1}), and good cycling stability, when employed as anode materials for LIB. Wu *et al.* recently obtained $Co_2V_2O_7$ hexagonal microplates *via* a hydrothermal synthesis method, and the materials showed a high reversible capacity of 866 mA h g^{-1} with a nearly 100% capacity retention after 150 cycles.[25] Similarly, Luo *et al.* prepared $Co_2V_2O_7$ nanosheets on graphene oxide templates, which also displayed a high reversible capacity of 962 mA h g^{-1} at 0.5 A g^{-1}, and an excellent rate capacity (441 mA h g^{-1} after 900 cycles at 5.0 A g^{-1}).[20] Besides $Co_2V_2O_7$, other cobalt vanadium oxides (CVO), such as CoV_2O_6 and $Co_3V_2O_8$, also exhibited good electrochemical performance when applied in both LIB anode materials and supercapacitors electrodes.[26–31] In particular, $Co_3V_2O_8$ with various morphologies (*e.g.*, macroporous nanosheets,[17] multilayered nanosheets,[26] hollow hexagons,[28] hollow microspheres,[32,33] sponge networks,[34] and nanowires[35,36]) have captivated loads of researchers because of their outstanding lithium storage properties. Although a few studies have manifested the promising electrochemical properties of $Co_3V_2O_8$, there are still many interesting areas unexplored, *e.g.*, the phase selection and electrochemical behavior of $Co_3V_2O_8$. Wu and co-works have successfully procured the samples of $Co_3V_2O_8$ micro-pencils for the first time,[37] and revealed the transformation from solid to hollow structures.

Center for Advanced Electric Energy Technologies (CAEET), School of Energy Science and Engineering, University of Electronic Science and Technology of China, Chengdu 611731, China. E-mail: mwu@uestc.edu.cn; gongfeng@u.nus.edu

† Electronic supplementary information (ESI) available. See DOI: 10.1039/c7ra03118a

‡ These two authors contributed equally to this work.

However, the solid $Co_3V_2O_8$ micro-pencils as high performance anodes have not been exploited and the formation process of the $Co_3V_2O_8$ micro-pencils have not been reported. On the other hand, the reported $Co_3V_2O_8$ generally have porous or hollow structures, which may limit the electrochemical behavior in several aspects when utilized as LIB anodes.

In this work, we successfully synthesized solid $Co_3V_2O_8$ particles *via* a facile and controllable hydrothermal method. The solid $Co_3V_2O_8$ particles could form either micro-plate or micro-pencil structures depending on the controlled reaction time. The energy dispersive X-ray spectroscopy (EDS) and XRD results demonstrated the formation and phase selection of $Co_3V_2O_8$. The SEM images of $Co_3V_2O_8$ materials obtained at different reaction time remarkably unveiled the evolution process of $Co_3V_2O_8$ micro-plates and micro-pencils. Through TEM and scanning TEM (STEM), the solid and hexagonal morphology were successfully observed. Simultaneously, the electrochemical performances of the $Co_3V_2O_8$ solid micro-pencils as the anode materials for LIB were further characterized. The corresponding results demonstrated that the $Co_3V_2O_8$ solid micro-pencils have a high specific capacity (initial discharge capacity of 1137 mA h g^{-1}), long life span (capacity of ~670 mA h g^{-1} after 330 cycles at 200 mA g^{-1}), and notable rate performance (capacity of 300 mA h g^{-1} at 2000 mA g^{-1}), which has great potential to be used as superior anode materials for lithium ion battery.

Experimental section

Sample preparation

Hydrothermal reactions were employed to synthesize $Co_3V_2O_8$ materials. For $Co_3V_2O_8$ micro-plates, 0.374 g of ammonium metavanadate was dissolved into 64 ml of deionized water at 80 °C. The solution was kept stirring until its color changed from pale yellow to green. Later, 0.08 g of LiOH H_2O was dissolved into the above solution, which changed to be transparent and colorless after several minutes. Subsequently, 0.14 g of $CoCl_2 \cdot 6H_2O$ was added into the mixed solution. After stirring for 10 min, the reddish brown transparent solution was transferred into a 100 ml Teflon-lined autoclave, tightly sealed, put into an oven and heated at 200 °C for 2 h. After cooling to room temperature in air, the final products were washed several times by deionized water and absolute ethanol, and dried at 80 °C for 6 h, followed by annealing in air atmosphere at 300 °C for 4 h. For $Co_3V_2O_8$ micro-pencils, all the conditions were kept same as used for $Co_3V_2O_8$ micro-plates synthesis, except the hydrothermal reaction time was changed to 8 h.

Materials characterization

XRD analysis of the prepared samples were performed on a Bruker-D8 Advanced X-ray Diffractometer (Cu Kα radiation: λ = 1.5406 Å) with a scanning speed of 2 deg min^{-1}. The morphologies of the prepared samples were observed by field-emission scanning microscope (FE-SEM, JSM-5900LV, JEOL). TEM, high resolution TEM (HRTEM) and scanning TEM (STEM) images were taken on a JEOL JEM-2100F microscope.

Electrochemical measurement

The electrochemical characterization was performed using 2032-type coin cells with two electrodes, assembled in an Ar-filled dry glove box with both the moisture and the oxygen content below 1 ppm. $Co_3V_2O_8$ and Li metal were employed as the working and counter electrodes, respectively. The working electrode was prepared with 80 wt% active materials ($Co_3V_2O_8$), 10 wt% conducting acetylene black, and 10 wt% PVDF. The slurry was pasted on a clean copper foil with a thickness of 0.2 mm. The loading density of the active material was about 1–2 mg cm^{-2}. 1 M $LiPF_6$ in ethyl carbonate (EC)–dimethyl carbonate (DMC) (1 : 1 by volume) was used as the electrolyte and a Celgard 2400 microporous membrane as the separator. Coin-type half-cells were tested at a voltage range of 0.01–3.0 V (*vs.* Li^+/Li) at room temperature, using a CT2001A LAND Cell test system. Cyclic voltammetry (CV) testing was carried out between 0.01 and 3 V (*vs.* Li/Li^+) at a scan rate of 0.5 mV s^{-1}.

Results and discussion

Structure and morphology

The EDS results and the XRD pattern of the obtained $Co_3V_2O_8$ micro-pencils are presented in Fig. 1, which demonstrate the composition and the successful phase selection of $Co_3V_2O_8$ micro-pencils. As shown in Fig. 1(a) and S1,† the EDS results indicate the $Co_3V_2O_8$ micro-pencils are composed of elements O, Co, and V. The detailed atomic ratio of Co/V is presented in Table S1† and reveals that the atomic ratio of Co/V is ~1.67, indicating the formation of $Co_3V_2O_8$. The XRD pattern in Fig. 1(b) shows that all the diffraction planes of the obtained $Co_3V_2O_8$ micro-pencils can be perfectly indexed to the cubic crystal structure of $Co_3V_2O_8$ (JCPDS no. 16-0675), which is consistent with other reported results.[19,26] Fig. S2† displays the XRD pattern of the $Co_3V_2O_8$ micro-pencils before annealing, which is notably compatible with the previous report of $Co_3V_2O_8 \cdot H_2O$.[37]

The SEM image in Fig. 2(a) clearly shows the morphology of the materials manufactured through the hydrothermal reaction for 6 h. A short pencil-like structure with a hexagonal cross section can be observed in the SEM image. The pencil-like $Co_3V_2O_8$ particles have a uniform micro-scale size distribution (*i.e.*, ~3 μm in the hexagonal side length and ~5 μm in the length). The $Co_3V_2O_8$ micro-pencils exhibited a solid morphology, different from the commonly reported hollow structure[28,38] is favorable for a high tap density and an enhanced volumetric lithium storage capacity when employed as LIB electrodes.[30,39] Both the TEM image with low magnification in Fig. 2(b) and the scanning TEM (STEM) image in Fig. 2(c) can also demonstrated the solid morphology and the hexagonal cross section of the obtained $Co_3V_2O_8$ micro-pencils. The high-resolution TEM image in Fig. 2(d) displays the measured inter-plane distance. The two inter-plane distance values, 0.252 nm and 0.209 nm, are in good agreement with the (311) (0.251 nm) and (400) (0.207 nm) lattice fringes of the cubic crystalline $Co_3V_2O_8$. These two planes also correspond to the main peaks in the XRD results of the cubic crystalline $Co_3V_2O_8$, as illustrated in Fig. 1(b).

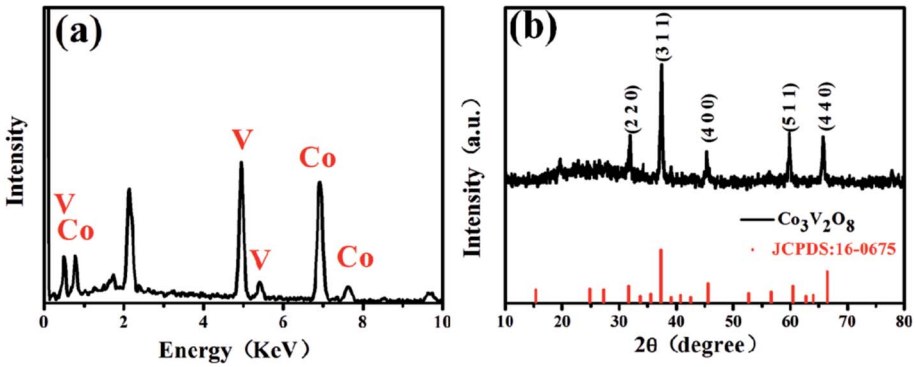

Fig. 1 EDS spectrum (a) and XRD pattern (b) of the obtained $Co_3V_2O_8$ micro-pencils. EDS spectrum indicates the obtained materials are composed of elements Co, V and O, while the XRD pattern demonstrates the obtained $Co_3V_2O_8$ micro-pencils have cubic crystal structures (JCPDS no. 16-0675).

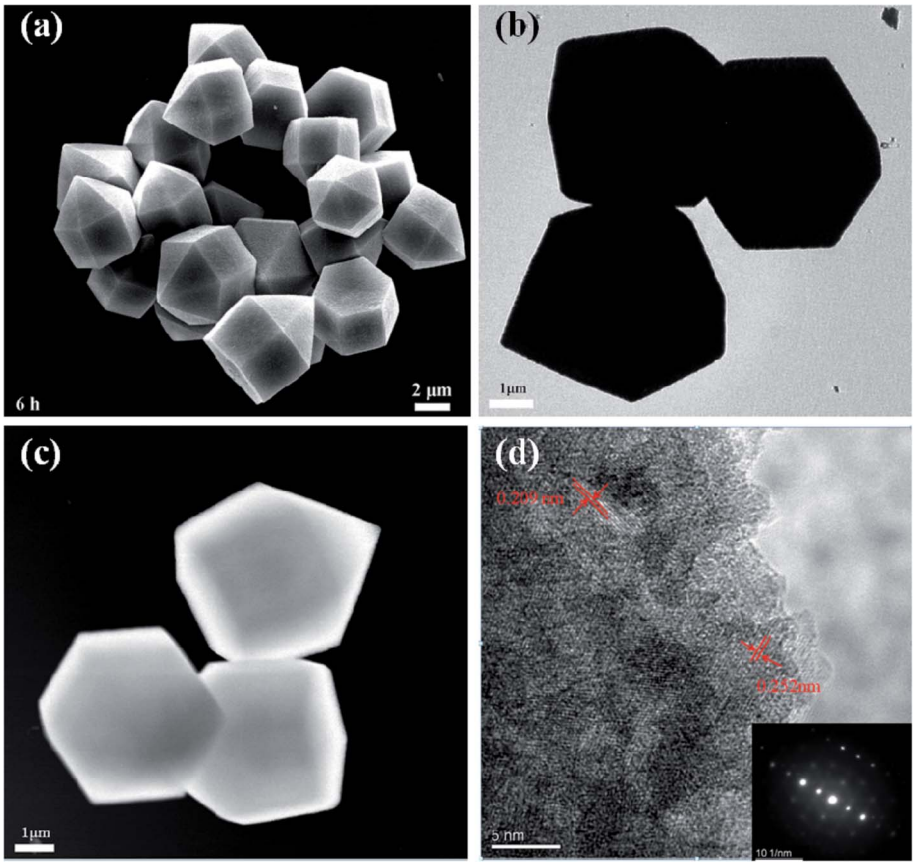

Fig. 2 (a) SEM image of $Co_3V_2O_8$ obtained for 6 h of hydrothermal reaction. The pencil-like structure with hexagonal cross section can be clearly observed. The $Co_3V_2O_8$ micro-pencils have uniform size distribution. (b) TEM image with low magnification of $Co_3V_2O_8$ micro-pencils. (c) STEM image of $Co_3V_2O_8$ micro-pencils. The TEM and STEM images indicate the solid feature of $Co_3V_2O_8$ micro-pencils. (d) High-resolution TEM image of $Co_3V_2O_8$ micro-pencils. The two measured inter-plane distances agree well with the (311) and (400) lattice fringes of the cubic crystalline $Co_3V_2O_8$, as shown in Fig. 1(b). The inset image in (d) is the corresponding SAED pattern.

Formation process of $Co_3V_2O_8$ micro-pencils

To understand the growth mechanism of the unique $Co_3V_2O_8$ micro-pencils, sample materials were collected at different reaction time during the hydrothermal process and their morphologies were characterized by SEM. As shown in Fig. 3, the morphologies of samples garnered at six stages during the hydrothermal reaction lucidly uncovered the formation process of the $Co_3V_2O_8$ micro-pencils. Meanwhile, a proposed formation process of the $Co_3V_2O_8$ micro-pencils and the corresponding schematic plot is presented in Fig. 4. At the initial stage, nano-scale spherical particles were formed (Fig. 3(a) and 4(a)) and gradually grow in both longitudinal and transverse directions to

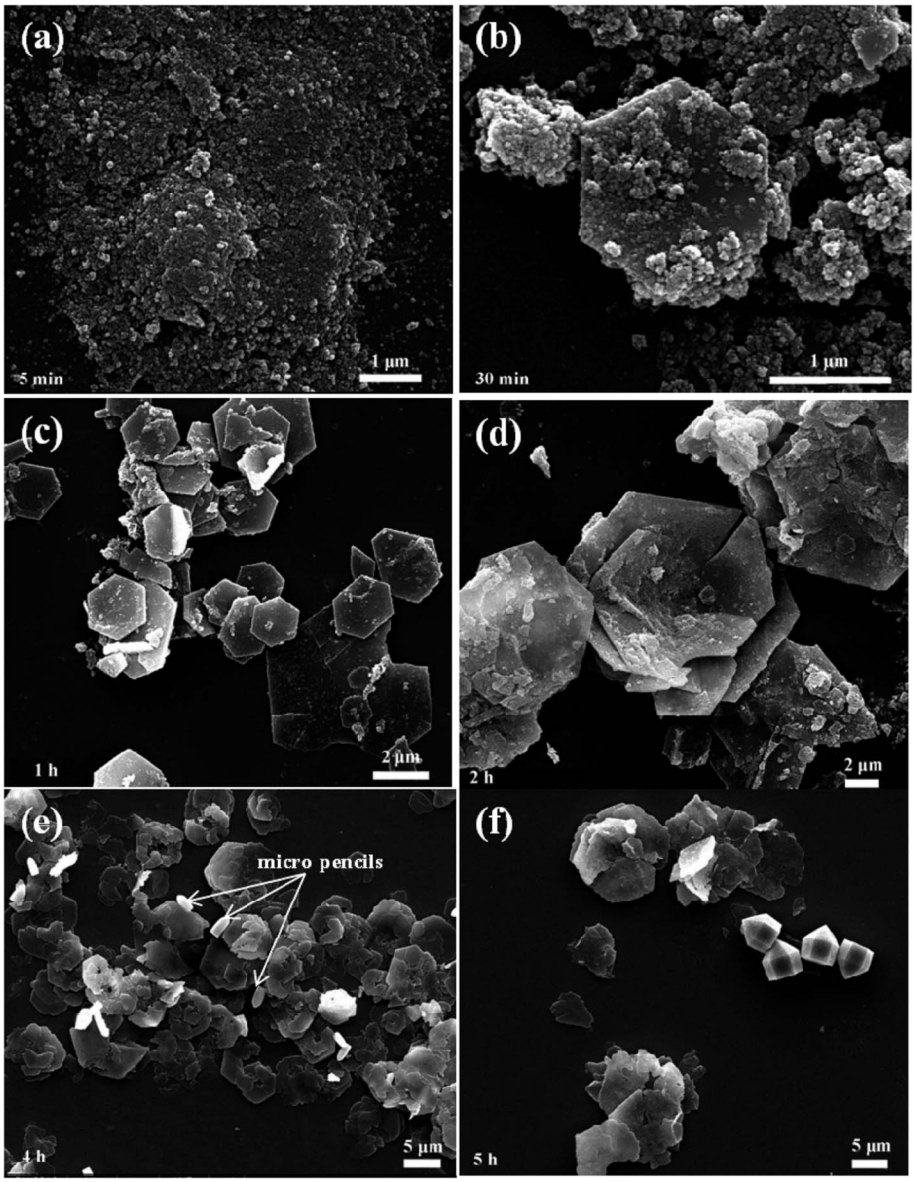

Fig. 3 Typical SEM images of the products obtained during the hydrothermal reaction at different stages: (a) 5 min, (b) 30 min, (c) 1 h, (d) 2 h, (e) 4 h, and (f) 5 h.

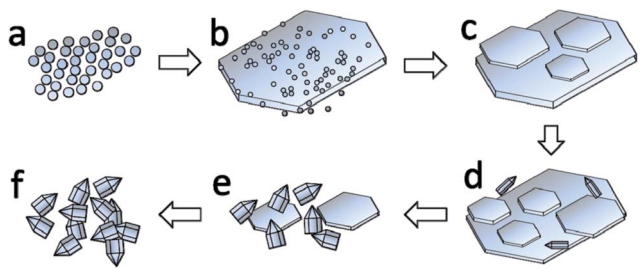

Fig. 4 Schematic plot of the potential evolution process of the $Co_3V_2O_8$ micro-pencils.

form microscale large clusters (Fig. 3(b) and 4(b)). As the reaction continues, hexagonal micro-plates are first observed, which are probably evolve from the nanoparticle clusters (Fig. 3(b)). When the reaction continues to 1 h, the hexagonal micro-plates probably undergo a crystallization process because of their more regular shape and smoother surface, as indicated by Fig. 3(c) and 4(c). The hexagonal micro-plates continue to grow both radially and longitudinally and larger diameter and thickness are obtained, which can be derived from Fig. 3(d). The hexagonal micro-plates start to peel off and the thinner sheets are observed when the reaction time is increased to 4 hours. More interestingly, micro-pencils begin to appear at this stage, as shown in Fig. 4(e) where both the micro-plates and micro-pencils can be clearly detected. After reaction for 5 h, the density of $Co_3V_2O_8$ micro-plates is remarkably decreased, while the $Co_3V_2O_8$ micro-pencils grow rapidly and attain the ultimate pencil-like morphology. When the reaction time is increased to 6 hours, the $Co_3V_2O_8$ micro-plates completely disappear, and only the

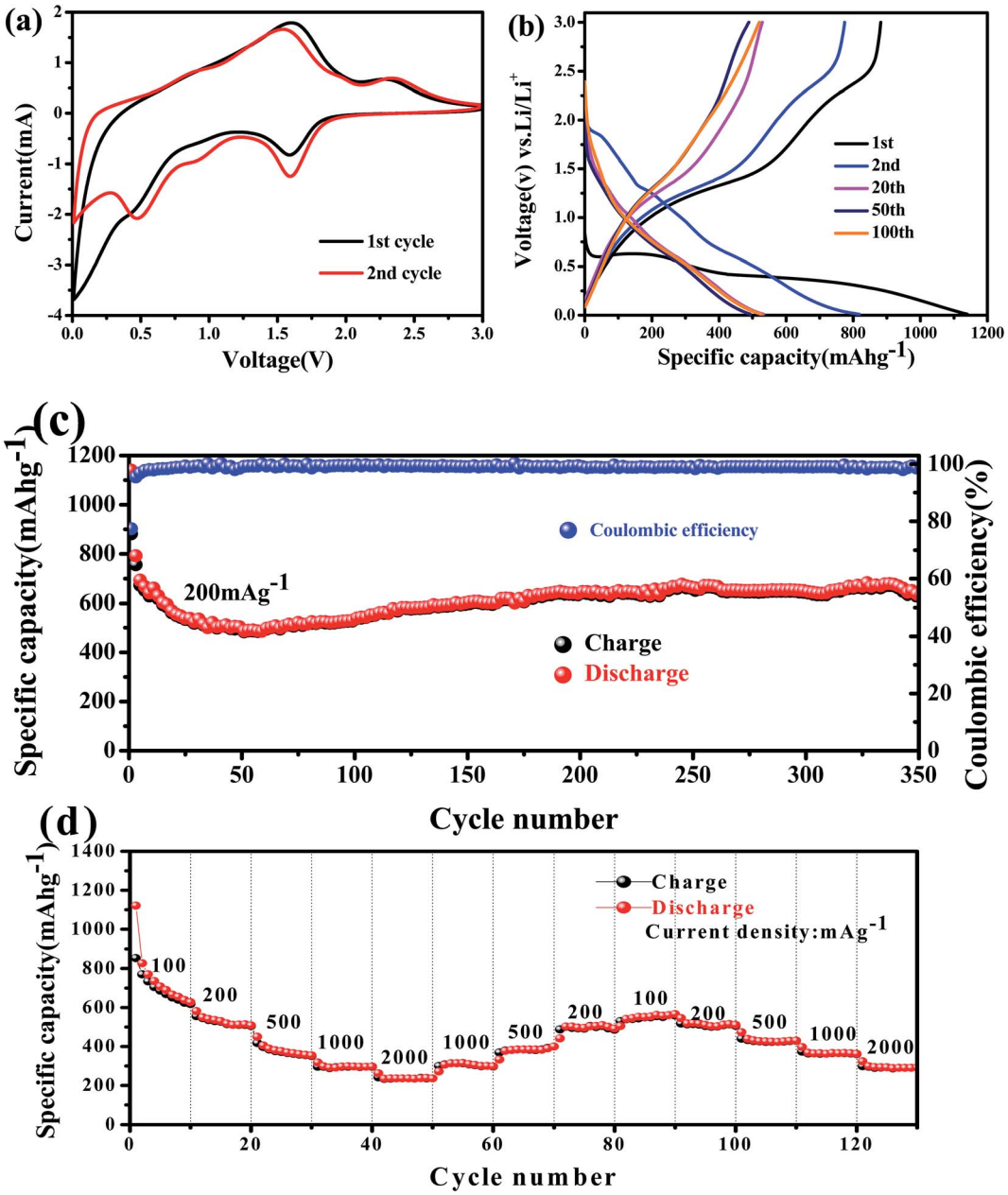

Fig. 5 Electrochemical properties of $Co_3V_2O_8$ micro-pencils: (a) cyclic voltammogram profiles of the $Co_3V_2O_8$ micro-pencils; (b) discharge and charge curves at the current density of 200 mA g^{-1}; (c) cycling property at the current density of 200 mA g^{-1}, and (d) rate performance at different current densities.

$Co_3V_2O_8$ micro-pencils exist in the final products, as shown in Fig. 2(a). Based on the SEM images in Fig. 3, it can be concluded that the morphology and size of the products are entirely controlled by the hydrothermal reaction time. Therefore, $Co_3V_2O_8$ with either micro-plate or micro-pencil structures can be successfully fabricated by easily controlling the reaction time. Moreover, we provided the XRD patterns of the samples collected at the six stages during the hydrothermal reaction in Fig. S3.†

Electrochemical properties

The electrochemical properties of the obtained $Co_3V_2O_8$ micro-pencils were characterized using 2032-type coin cells. The cyclic voltammograms (CVs) of the $Co_3V_2O_8$ micro-pencils are presented in Fig. 5(a), which was obtained at a scan rate of 0.5 mV s^{-1} and in the potential window of 3 V to 0.01 V. In the first cathodic sweep, three reduction peaks were found at 1.59 V, 0.49 V, and 0.02 V, respectively, which could be assigned to the reduction of $Co_3V_2O_8$ to CoO ($Co_3V_2O_8 \rightarrow 3CoO + V_2O_5$), the further reduction of CoO to metallic Co ($CoO + 2Li^+ + 2e^- \rightarrow Co + Li_2O$), and the formation of Li–Co alloys,[40] respectively. Meanwhile, the reductions were accompanied with the lithiation of V_2O_5 ($V_2O_5 + xLi^+ + xe^- \rightarrow Li_xV_2O_5$), and the further insertion of Li ions into $Li_xV_2O_5$ ($Li_xV_2O_5 + yLi^+ + ye^- \rightarrow Li_{x+y}V_2O_5$). During the reverse scan, two oxidation peaks were

conspicuously observed at 1.65 V and 2.35 V. The lower oxidation peak at 1.65 V was owing to the de-alloying of Li–Co, Li^+ extraction from $Li_{x+y}V_2O_5$, and the oxidation of Co to CoO. The higher peak at 2.35 V was ascribed to the further extraction of Li ions from $Li_xV_2O_5$, and the oxidation of CoO to $Co_3V_2O_8$.

Fig. 5(b) displays the galvanostatic discharge and charge results at the 1st, 2nd, 20th, 50th, and 100th cycle of the $Co_3V_2O_8$ micro-pencil anode at a current density of 200 mA g^{-1} and a voltage range of 0.01 V to 3 V (*vs.* Li^+/Li). In the first discharge curve, the potential sharply drops to 0.55 V, then reaches a plateau, and dwindle till reaching a specific capacity of 1137 mA h g^{-1}. The first charge capacity of 882 mA h g^{-1} is obtained, therefore, the coulombic efficiency of 77% is calculated. The higher initial discharge capacity is caused by the interfacial lithium storage, in which the electrolyte decomposes to form a solid electrolyte interphase (SEI) layer.[41] The Faraday's law of electrolysis can be used to estimate the amount of Li atoms per formula unit in lithiation and delithiation processes, which is expressed as below:[42]

$$m = \left(\frac{Q}{F}\right)\left(\frac{M}{n}\right) \quad (1)$$

where m is the mass of the active materials in electrode in grams (*i.e.* $Co_3V_2O_8$ in this work), Q is the total electric charge passed through the electrode in coulombs, M is the molar mass of the active materials in grams per mole, n is the number of intercalated/deintercalated Li atoms in the electrodes, and F is the Faraday constant, which is 96 485 C mol^{-1}. Thus, the theoretical capacity of an active material can be derived from eqn (1) and described as:

$$C_{\text{theory}} = \frac{nF}{M \times 3600} \quad (2)$$

where C_{theory} is the theoretical specific capacity of the active material in the unit of mA h g^{-1}. As we measured the specific capacity of the $Co_3V_2O_8$ micro-pencils, the number of Li atoms per formula unit in lithiation and delithiation can be calculated as 16.1 and 11.2 according to eqn (2), which is close but slightly lower than that of the previous study.[19]

Fig. 5(c) presents the cycling performance of the $Co_3V_2O_8$ micro-pencils at the current density of 200 mA g^{-1}. The specific capacity decreases progressively from the initial capacity of 1137 mA h g^{-1} with the increase of cycles, followed by a slow rise of the specific capacity after the 50th cycle and reached 670 mA h g^{-1} at 330th. Even after 350 cycles, the capacity still maintained a plateau at ~620 mA h g^{-1}. This similar interesting change behavior of the capacity has also been shown in some other studies.[26,28] However, the mechanism is not clear and therefore further studies are still required. As shown in Fig. 5(c), after the initial discharge/charge, the discharge and charge capacities overlap well with each other, indicating an superb capacity reversibility. The capacity retention is further demonstrated by the calculated coulombic efficiency, which maintain at almost 100% after the first cycle. The discharge capacity was measured at different current densities from 100 to 2000 mA g^{-1}, as presented in Fig. 5(d). The average discharge capacities of at the current density of 100, 200, 500, 1000 and 2000 mA g^{-1} are stabilized at 700, 550, 420, 350, and 300 mA h g^{-1}, respectively, regardless of change direction of the current density, thus revealing the stability of the $Co_3V_2O_8$ micro-pencils in the rate performance. The overlaps between the discharge and charge capacities indicate the high capacity retention (~100%) during the rate performance.

Conclusions

In summary, we have demonstrated a facile hydrothermal approach to synthesize $Co_3V_2O_8$ solid micro-particles with controllable morphology. Through the XRD, SEM, TEM and STEM, pure phase $Co_3V_2O_8$ solid micro-plates and micro-pencils are thoroughly scrutinized. When evaluated as anode materials for lithium ion battery, the $Co_3V_2O_8$ solid micro-pencils exhibit satisfactory electrochemical performance: high Li storage capacity (initial discharge capacity of 1137 mA h g^{-1} at 200 mA g^{-1}), superior cycling performances (capacity of ~620 mA h g^{-1} after 350 cycles at 200 mA h^{-1}), and notable rate capability (capacity of 300 mA h g^{-1} at 2000 mA g^{-1}). The present study demonstrates the potential of $Co_3V_2O_8$ solid micro-pencils as the promising anode materials for LIB. Hydrothermal approach can also be employed for synthesizing other mixed transition metal oxides for diverse energy storage applications. Nevertheless, further studies should be conducted to shed light on the formation of the $Co_3V_2O_8$ with different morphology, and to ameliorate the electrochemical performances of $Co_3V_2O_8$ related materials.

Acknowledgements

The authors would like to appreciate the financial support from National Natural Science Foundation of China (201503036, 51602038), Sichuan Science and Technology Support Program (2015GZ0130, 2016000156, 2015GZ0132, 2016JY0183) and the Fundamental Research Funds for the Central Universities (ZYGX2015KYQD030).

References

1 W. W. Lee and J.-M. Lee, *J. Mater. Chem. A*, 2014, **2**(6), 1589–1626.
2 Y. S. Wu, L. Zhan, K. T. Huang, H. J. Wang, H. Yu, S. Q. Wang, F. Peng and C. Y. Lai, *J. Alloys Compd.*, 2016, **684**, 47–54.
3 B. Liu, P. F. Yan, W. Xu, J. M. Zheng, Y. He, L. L. Luo, M. E. Bowden, C. M. Wang and J. G. Zhang, *Nano Lett.*, 2016, **16**(8), 4932–4939.
4 K. Zhao, M. Wen, Y. Dong, L. Zhang, M. Yan, W. Xu, C. Niu, L. Zhou, Q. Wei, W. Ren, X. Wang and L. Mai, *Adv. Energy Mater.*, 2017, **7**(6), 1601582.
5 P. Poizot, S. Laruelle, S. Grugeon, L. Dupont and J. M. Tarascon, *Nature*, 2000, **407**(6803), 496–499.
6 Y. Wang and G. Z. Cao, *Adv. Mater.*, 2008, **20**(12), 2251–2269.
7 H. B. Wu, J. S. Chen, H. H. Hng and X. W. Lou, *Nanoscale*, 2012, **4**(8), 2526–2542.
8 P. Roy and S. K. Srivastava, *J. Mater. Chem. A*, 2015, **3**(6), 2454–2484.

9 A. Manthiram, A. V. Murugan, A. Sarkar and T. Muraliganth, *Energy Environ. Sci.*, 2008, **1**(6), 621–638.
10 L. Zhou, H. Xu, H. Zhang, J. Yang, S. B. Hartono, K. Qian, J. Zou and C. Yu, *Chem. Commun.*, 2013, **49**(77), 8695–8697.
11 H. Zhang, X. Sun, X. Huang and L. Zhou, *Nanoscale*, 2015, **7**(7), 3270–3275.
12 C. Yuan, H. B. Wu, Y. Xie and X. W. Lou, *Angew. Chem., Int. Ed.*, 2014, **53**(6), 1488–1504.
13 C. Z. Yuan, H. B. Wu, Y. Xie and X. W. Lou, *Angew. Chem., Int. Ed.*, 2014, **53**(6), 1488–1504.
14 J. X. Zhu, T. Zhu, X. Z. Zhou, Y. Y. Zhang, X. W. Lou, X. D. Chen, H. Zhang, H. H. Hng and Q. Y. Yan, *Nanoscale*, 2011, **3**(3), 1084–1089.
15 L. Zhou, D. Zhao and X. W. Lou, *Adv. Mater.*, 2012, **24**(6), 745–748.
16 L. J. Fu, H. Liu, C. Li, Y. P. Wu, E. Rahm, R. Holze and H. Q. Wu, *Solid State Sci.*, 2006, **8**(2), 113–128.
17 L. Zhang, K. Zhao, Y. Luo, Y. Dong, W. Xu, M. Yan, W. Ren, L. Zhou, L. Qu and L. Mai, *ACS Appl. Mater. Interfaces*, 2016, **8**(11), 7139–7146.
18 Z. Yin, Y. Xiao, X. Wang, W. Wang, D. Zhao and M. Cao, *Nanoscale*, 2016, **8**(1), 508–516.
19 V. Soundharrajan, B. Sambandam, J. Song, S. Kim, J. Jo, S. Kim, S. Lee, V. Mathew and J. Kim, *ACS Appl. Mater. Interfaces*, 2016, **8**(13), 8546–8553.
20 Y. Luo, X. Xu, Y. Zhang, C.-Y. Chen, L. Zhou, M. Yan, Q. Wei, X. Tian and L. Mai, *ACS Appl. Mater. Interfaces*, 2016, **8**(4), 2812–2818.
21 Y. Luo, X. Xu, X. Tian, Q. Wei, M. Yan, K. Zhao, X. Xu and L. Mai, *J. Mater. Chem. A*, 2016, **4**(14), 5075–5080.
22 F. Y. Cheng and J. Chen, *J. Mater. Chem.*, 2011, **21**(27), 9841–9848.
23 H. Ben Yahia, M. Shikano and Y. J. Yamaguchi, *Power Sources*, 2016, **320**, 43–48.
24 C. Tang, J. Zhu, X. Wei, L. He, K. Zhao, C. Xu, L. Zhou, B. Wang, J. Sheng and L. Mai, *Energy Storage Materials*, 2017, **7**, 152–156.
25 F. Wu, C. Yu, W. Liu, T. Wang, J. Feng and S. Xiong, *J. Mater. Chem. A*, 2015, **3**(32), 16728–16736.
26 G. Yang, H. Cui, G. Yang and C. Wang, *ACS Nano*, 2014, **8**(5), 4474–4487.
27 G. Z. Yang, H. Cui, G. W. Yang and C. X. Wang, *ACS Nano*, 2014, **8**(5), 4474–4487.
28 F. Wu, S. Xiong, Y. Qian and S.-H. Yu, *Angew. Chem., Int. Ed.*, 2015, **54**(37), 10787–10791.
29 Y. Zhang, Y. Liu, J. Chen, Q. Guo, T. Wang and H. Pang, *Sci. Rep.*, 2014, **4**, 5687.
30 S. B. Ni, J. J. Ma, J. C. Zhang, X. L. Yang and L. L. Zhang, *J. Power Sources*, 2015, **282**, 65–69.
31 L. Zhang, K. N. Zhao, Y. Z. Luo, Y. F. Dong, W. W. Xu, M. Y. Yan, W. H. Ren, L. Zhou, L. B. Qu and L. Q. Mai, *ACS Appl. Mater. Interfaces*, 2016, **8**(11), 7139–7146.
32 G. X. Gao, S. Y. Lu, B. T. Dong, Y. Xiang, K. Xi and S. J. Ding, *J. Mater. Chem. A*, 2016, **4**(17), 6264–6270.
33 Y. Z. Luo, X. Xu, X. C. Tian, Q. L. Wei, M. Y. Yan, K. N. Zhao, X. M. Xu and L. Q. Mai, *J. Mater. Chem. A*, 2016, **4**(14), 5075–5080.
34 V. Soundharrajan, B. Sambandam, J. Song, S. Kim, J. Jo, S. Kim, S. Lee, V. Mathew and J. Kim, *ACS Appl. Mater. Interfaces*, 2016, **8**(13), 8546–8553.
35 Y. Li, L. Kang, L. B. Kong, M. C. Liu, X. X. Wang and W. B. Zhang, *RSC Adv.*, 2016, **6**(43), 36418–36424.
36 M. C. Liu, L. B. Kong, L. Kang, X. H. Li, F. C. Walsh, M. Xing, C. Lu, X. J. Ma and Y. C. Luo, *J. Mater. Chem. A*, 2014, **2**(14), 4919–4926.
37 F. Wu, S. Xiong, Y. Qian and S. H. Yu, *Angew. Chem.*, 2015, **54**(37), 10787–10791.
38 Y. Luo, X. Xu, X. Tian, Q. Wei, M. Yan, K. Zhao, X. Xu and L. Mai, *J. Mater. Chem. A*, 2016, **4**(14), 5075–5080.
39 L. Wu, S. N. Shi, X. P. Zhang, J. Q. Liu, D. Chen, H. Ding and S. K. Zhong, *Mater. Lett.*, 2015, **152**, 228–231.
40 V. Soundharrajan, B. Sambandam, J. Song, S. Kim, J. Jo, S. Kim, S. Lee, V. Mathew and J. Kim, *ACS Appl. Mater. Interfaces*, 2016, **8**(13), 8546–8553.
41 N. Liu, Z. D. Lu, J. Zhao, M. T. McDowell, H. W. Lee, W. T. Zhao and Y. Cui, *Nat. Nanotechnol.*, 2014, **9**(3), 187–192.
42 R. G. Ehl and A. J. Ihde, *J. Chem. Educ.*, 1954, **31**(5), 226.